A Polarized Temporal Network Model to Study the Spread of Recurrent Epidemic Diseases in a Partially Vaccinated Population

Kathinka Frieswijk, *Student Member, IEEE,* Lorenzo Zino, *Member, IEEE,* and Ming Cao, *Fellow, IEEE*

Abstract—Motivated by massive outbreaks of COVID-19 that occurred even in populations with high vaccine uptake, we propose a novel multi-population temporal network model for the spread of recurrent epidemic diseases. We study the effect of human behavior, testing, and vaccination campaigns on infection prevalence and local outbreak control. Our modeling framework decouples a vaccine's effectiveness in protecting against transmission and severe symptom development. Additionally, it captures the polarizing effect of vaccination decisions and homophily, i.e., people's tendency to interact with like-minded individuals. Through a mean-field approach, we analytically derive the epidemic threshold and, under further assumptions, we compute the endemic equilibrium. Our results show that while vaccination campaigns are highly beneficial in reducing pressure on hospitals, they may also facilitate resurgent outbreaks, particularly in the absence of effective testing campaigns. Subsequently, we employ numerical simulations to confirm and extend our theoretical findings to more realistic scenarios. Our analytical and numerical results demonstrate that vaccination programs are crucial, but as a sole control measure, they are not sufficient to achieve disease eradication without employing massive testing campaigns or relying on the population's responsibility. Furthermore, we show that homophily impedes local outbreak control, highlighting the peril of a polarized network structure.

Index Terms—Epidemics, homophily, network dynamics, temporal network, vaccination

1 Introduction

In response to the COVID-19 pandemic that emerged in Wuhan, China, in December 2019, an unprecedented effort has been made toward developing a vaccine in record time [2]. Although current COVID-19 vaccines are highly effective against severe symptom development—thereby reducing the number of deaths and pressure on hospitals—they provide limited protection against transmission, especially concerning the new variants that became dominant in 2021–22 [3], [4]. As massive outbreaks have occurred in populations with high vaccination coverage [4], it begs the following question: *is it possible to eradicate the pandemic by solely relying on vaccination programs? If not, could testing campaigns and human behavior be pivotal to achieving this goal?*

To study the dynamics of the spread of a disease, it is common practice to use mathematical modeling. In particular, epidemic models on networks have emerged as a framework to successfully incorporate the mobility patterns of human-to-human interaction that serve as a pathway for the conveyance of disease [5], [6], [7], [8], [9]. Among the reasons for their success, network epidemic models allow for the development of tractable and analytically rigorous mathematical frameworks to study the spread of epidemic diseases [10], [11], [12] and to construct policies to control them [13]. Moreover, they are open to several extensions toward the inclusion of real-world features, e.g., by adding a state of awareness in which individuals adopt preventive behavior [14]. Previously, network epidemic models were successfully employed to study the effect of vaccination campaigns [15], [16], [17]. Recently, they have been applied to study the COVID-19 pandemic, to support governments in designing effective control strategies [18], [19], [20], [21].

Motivated by the questions formulated above, we propose a multi-population network model to investigate the roles of vaccination programs, testing campaigns, and human behavior in the spread of recurrent epidemic diseases, which include infections caused by fast-mutating viruses (e.g., influenza viruses). Our model extends the standard susceptible–infected–susceptible (SIS) model by incorporating two distinct compartments for mildly symptomatic and severely symptomatic infected individuals, where the latter are in quarantine. The proposed framework, referred to as the susceptible–infected–quarantined–susceptible (SIQS) model, includes a responsibility level, reflecting the extent to which mildly symptomatic individuals do not overlook their symptoms and adhere to preventive measures to avoid transmission. Within our modeling framework, we investigate the co-evolution of the progression of the epidemic and the network of human-to-human interactions, utilizing a network formation process that is based on continuous-time activity-driven networks [22], [23]. We evaluate two measures to control the spreading of the infection. First, we consider *vaccination programs*, where we assume that a fixed part of the population is vaccinated. The effect of vaccination is modeled through the parsimonious addition of two distinct parameters to elegantly decouple effects on

• *Some preliminary results have appeared in [1], in the form of a conference paper. KF and MC are with the Engineering and Technology Institute Groningen, University of Groningen, Groningen, The Netherlands, e-mail:* {k.frieswijk,m.cao}rug.nl. *LZ was with the Engineering and Technology Institute Groningen, University of Groningen, Groningen, The Netherlands; currently, he is with the Department of Electronics and Telecommunications, Politecnico di Torino, Torino, Italy, e-mail:* lorenzo.zino@polito.it. *The work was partially supported by the European Research Council (ERC–CoG–771687).*

reducing contagion and protecting against severe symptoms. Second, we consider *testing campaigns*, which identify and isolate mildly symptomatic infected individuals.

Despite a consensus among the scientific community that vaccines approved by public health authorities are effective and safe, the debate on whether to vaccinate is very polarizing, and individuals with similar attitudes toward vaccination prefer to interact with one another [24], [25], [26], [27]. Here, we investigate the effect that this phenomenon of *homophily* has on the spread of epidemic diseases by developing a mathematical model that encapsulates such a phenomenon. Specifically, we expand our preliminary model [1] by embedding it in a multi-population network scenario that accounts for the polarizing effect of the vaccination decision, capturing the tendency of individuals to establish more interactions with like-minded people.

Employing a mean-field approach on a large population [28], [29], we perform a theoretical analysis of our network model and derive a closed-form expression for the epidemic threshold. Such an analytical expression sheds light on the roles of network polarization, population responsibility, and vaccination in controlling local outbreaks. Next, we analyze the system behavior above the epidemic threshold, characterizing the endemic equilibrium (EE) under some additional assumptions. Finally, we numerically investigate a generalization of our SIQS model that encapsulates (temporary) natural immunity after recovery, with parameters calibrated on the COVID-19 pandemic.

Our theoretical results suggest that—while vaccination is beneficial in reducing the number of deaths—its role in controlling local outbreaks is not straightforward and depends on individuals' responsibility levels and the characteristics of both the vaccine and the infection. Hence, in some cases, relying only on vaccination could act as a double-edged sword, hindering the complete eradication of the disease. To compensate for this, the simultaneous implementation of massive testing campaigns is essential. Our simulations provide further insights into the role of human behavior. Notably, they suggest that responsibility is vital; for low responsibility levels, it is impossible to eradicate the infection without employing massive testing campaigns. Furthermore, both our theoretical and numerical results show that a high degree of homophily facilitates the spreading of a disease. Thus, our results underline the peril of polarization, with clusters of individuals who disregard vaccines and the use of protective measures.

The rest of the paper has the following organization. Section 2 introduces the notation and some mathematical preliminaries. Section 3 illustrates our modeling framework. Next, Section 4 presents the model analysis and main theoretical results. Subsequently, Section 5 discusses our numerical findings, and the paper is concluded in Section 6.

2 Notation and Preliminaries

Here, we gather some notational conventions and present classical properties of Poisson processes used in the rest of the paper (see [30], [31] for more details on stochastic processes).

Let $\mathbb{R}_{\geq 0}$ and $\mathbb{R}_{>0}$ denote the sets of non-negative and strictly positive real numbers, respectively. Let $\mathbb{Z}_{\geq 0}$ denote the set of non-negative integers. Given a function $x(t)$ with $t \in \mathbb{R}_{\geq 0}$, we define $x(t^+) = \lim_{s \searrow t} x(s)$, and $x(t^-) = \lim_{s \nearrow t} x(s)$. Given an event E, we denote by $\mathbb{P}[E]$ the probability that E occurs. Given a random variable X, we denote its expected value by $\mathbb{E}[X]$.

Definition 1. *A Poisson clock with (possibly time-varying) rate $\gamma(t)$ is a continuous-time stochastic process, represented by its counting process $N(t) \in \mathbb{Z}_{\geq 0}$. Specifically, $N(t)$ is a non-decreasing function that satisfies*

$$\mathbb{P}[N(t+\Delta t) - N(t) = 1] = \int_t^{t+\Delta t} \gamma(t)\,\mathrm{d}t + o(\Delta t)\,, \quad (1)$$

for $\Delta t \in \mathbb{R}_{>0}$, where the Landau little-o notation $o(\Delta t)$ is associated with the limit $\Delta t \searrow 0$; hence, $\lim_{\Delta t \searrow 0} \mathbb{P}[N(t+\Delta t) - N(t) = 1]/\Delta t = \gamma(t)$. If $N(t)$ has an increment at time $t \in \mathbb{R}_{\geq 0}$, we say that the clock ticks at time t.

Proposition 1 (Flow aggregation)**.** *Let E be an event triggered by the first tick of a set of independent Poisson clocks with rates $\gamma_1(t), \ldots, \gamma_\ell(t)$. Then, event E can be equivalently described as triggered by a Poisson clock with a rate of $\gamma_E(t) := \sum_{h=1}^{\ell} \gamma_h(t)$.*

Proposition 2 (Flow splitting)**.** *Let E be an event that occurs with probability $p \in [0,1]$ if a Poisson clock with a rate of $\gamma(t)$ ticks, where p is independent of the Poisson clock. Then, E occurs if triggered by a Poisson clock with a rate equal to $\gamma_E := p\gamma$.*

Definition 2. *A continuous-time stochastic process $X(t)$ with the state space $\mathcal{A}$ is a Markov process if for any states $h, k \in \mathcal{A}$, the transition from h to k is triggered by an independent Poisson clock with a rate of $q_{hk}(t)$. The transition rates are gathered in the transition rate matrix $Q(t) \in \mathbb{R}^{|\mathcal{A}|\times|\mathcal{A}|}$.*

3 Model

We extend the traditional network SIS model [9] by separating infected individuals into two distinct compartments: i) *infectious* individuals, who are untested and mildly symptomatic, and ii) *quarantined* individuals, who are in isolation due to a positive test result or because they are severely symptomatic. In the rest of this section, we will present all the details of our multi-population SIQS model.

3.1 Multi-population model

We consider a population of n individuals $\mathcal{V} = \{1, \ldots, n\}$, where the individuals are connected through a time-varying undirected network $\mathcal{G}(t) := (\mathcal{V}, \mathcal{E}(t))$, which evolves in continuous time $t \in \mathbb{R}_{\geq 0}$. Each $j \in \mathcal{V}$ has a health state $X_j(t) \in \{\mathrm{S}, \mathrm{I}, \mathrm{Q}\}$, where S, I, and Q denote a susceptible, infectious, and quarantined infected health state, respectively.

According to their vaccination status, individuals are partitioned into two subpopulations: i) a fully *vaccinated* subpopulation of size $n_{\mathrm{v}} \in \{1, \ldots, n-1\}$, and ii) a *non-vaccinated* subpopulation of size $n - n_{\mathrm{v}}$. Without any loss of generality, we assume that individuals $\mathcal{V}_{\mathrm{v}} := \{1, \ldots, n_{\mathrm{v}}\}$ belong to the first subpopulation, while individuals $\mathcal{V}_{\mathrm{n}} := \{n_{\mathrm{v}} + 1, \ldots, n\}$ belong to the second one. Let $v := \frac{n_{\mathrm{v}}}{n} \in (0,1)$ be the *vaccination coverage* of the population. Thus, $(\mathcal{V}, v)$ fully characterizes the multi-population model.

Transmission of the disease transpires via pairwise interactions at close distances, which occur at a timescale comparable with the epidemic spreading. Such an interaction

is henceforth named *contact*. These contact moments are modeled via a time-varying undirected network $\mathcal{G}(t) := (\mathcal{V}, \mathcal{E}(t))$, with $t \in \mathbb{R}_{\geq 0}$, where the time-varying edge set $\mathcal{E}(t)$ denotes the close interactions between individuals at time t. Specifically, $\{j, k\} \in \mathcal{E}(t)$ if and only if individuals j and k interact in close proximity (that is, they have contact) at time t. As is the case for many infectious diseases, the network formation process and the disease transmission process not only evolve at comparable timescales, but they are also deeply intertwined, as we detail in the following.

3.2 Network formation

To reflect an individual's tendency to interact with like-minded individuals from their subpopulation, we introduce a parameter $\theta \in [0, 1)$. Interactions take place stochastically, inspired by activity-driven networks in continuous time [32]. Each individual has a unit rate Poisson clock that ticks independently of other individuals' clocks. When the clock ticks, the individual initiates an interaction. Specifically, if the clock associated with $j \in \mathcal{V}$ ticks at time $t \in \mathbb{R}_{\geq 0}$, then j activates and interacts with another individual k that is chosen according to a probabilistic rule: with probability θ, k is selected uniformly at random from j's subpopulation, while with probability $1 - \theta$, k is chosen uniformly at random from the entire population. Hence, positive values of θ capture the presence of homophily in the population, similar to [33].

Whether the individuals have close contact depends on the health state and responsibility levels of the individuals involved. In particular, we assume that any quarantined individual j ($X_j(t) = \mathrm{Q}$) does not interact with others at a close distance. Infectious individuals with mild symptoms ($j : X_j(t) = \mathrm{I}$) can be near others, however. Whether they have contact with others depends on the individuals' level of responsibility. Specifically, let $\sigma_j \in [0, 1]$ denote the responsibility of individual $j \in \mathcal{V}$. If an infected individual j is mildly symptomatic ($X_j(t) = \mathrm{I}$), they refrain from having contact with probability σ_j; with probability $1 - \sigma_j$, they disregard their symptoms and do not maintain physical distance while interacting. We assume that the decision to maintain physical distance or not is made independently of the past and other individuals.

To be precise, if a susceptible individual j ($X_j(t^-) = \mathrm{S}$) activates and selects a mildly symptomatic infectious individual k ($X_k(t^-) = \mathrm{I}$) at time $t^- \in \mathbb{R}_{\geq 0}$, then they are in contact at time t with a probability of $1 - \sigma_k$; if k is susceptible ($X_k(t^-) = \mathrm{S}$), then they always have contact at time t. If a mildly symptomatic infectious individual j ($X_j(t^-) = \mathrm{I}$) activates and interacts with a susceptible individual k ($X_k(t^-) = \mathrm{S}$) at time $t^- \in \mathbb{R}_{\geq 0}$, then they have contact at time t with probability $1 - \sigma_j$; if k is mildly symptomatic too ($X_k(t^-) = \mathrm{I}$), then they have contact at time t with probability $(1 - \sigma_j)(1 - \sigma_k)$ (i.e., if they both ignore the symptoms). Finally, we recall our assumption that quarantined individuals ($j : X_j(t^-) = \mathrm{Q}$) always maintain distance, and thus, they do not establish any contact. If individuals j and k are in contact at time t, then the ephemeral edge $\{j, k\}$ is included in the set $\mathcal{E}(t)$, and subsequently, instantaneously removed from the edge set $\mathcal{E}(t^+)$.

TABLE 1: Model and control parameters.

$n \in \mathbb{N}$	population size
$t \in \mathbb{R}_{\geq 0}$	time
$X_j(t)$	health state of individual $j \in \mathcal{V}$ at time t
$(\mathcal{V}, \mathcal{E}(t))$	contact network (interactions in close proximity)
$v \in (0, 1)$	vaccination coverage
$\mathcal{V}_{\mathrm{v}} \subset \mathcal{V}$	vaccinated subpopulation
$\mathcal{V}_{\mathrm{n}} \subset \mathcal{V}$	non-vaccinated subpopulation
$\sigma_j \in [0, 1]$	responsibility level of individual $j \in \mathcal{V}$
$\sigma_{\mathrm{v}} \in [0, 1]$	responsibility level of vaccinated individuals
$\sigma_{\mathrm{n}} \in [0, 1]$	responsibility level of non-vaccinated individuals
$\lambda \in (0, 1]$	per-contact infection probability
$p_{\mathrm{q}} \in [0, 1]$	probability of severe illness
$\beta \in \mathbb{R}_{>0}$	recovery rate
$\gamma_{\mathrm{t}} \in [0, 1]$	effectiveness of vaccine against transmission
$\gamma_{\mathrm{q}} \in [0, 1]$	effectiveness of vaccine against severe illness
$\tau \in \mathbb{R}_{\geq 0}$	testing rate
$\theta \in [0, 1)$	homophily level with respect to interactions

3.3 Disease transmission and control

The evolution of the health state of each individual $j \in \mathcal{V}$ is governed by the following two natural mechanisms (contagion and recovery) and free testing campaigns, where we interpret the latter's intensity as a control input.

Contagion. Transmission of the infection occurs through close contact. Here, we assume that a positive vaccination status reduces i) the risk of becoming infected and ii) the risk of developing severe illness if infected. To model these effects, we introduce two parameters: $\gamma_{\mathrm{t}} \in [0, 1]$ and $\gamma_{\mathrm{q}} \in [0, 1]$, respectively. Specifically, the contagion process acts as follows. If a susceptible individual j ($X_j(t^-) = \mathrm{S}$) has contact with a mildly symptomatic infectious individual k ($X_k(t^-) = \mathrm{I}$) at time t, so $\{j, k\} \in \mathcal{E}(t)$, then j becomes infected with *per-contact infection probability* $\lambda \in (0, 1]$ if j is not vaccinated. If j is vaccinated, such a probability is reduced to $\lambda(1 - \gamma_{\mathrm{t}}) \in [0, 1]$.

If the infection is transmitted, individual j will either move to health state I or to Q. Specifically, the individual will become severely symptomatic ($X_j(t^+) = \mathrm{Q}$) with probability $p_{\mathrm{q}} \in [0, 1]$ if j is not vaccinated, while this probability is reduced to $p_{\mathrm{q}}(1 - \gamma_{\mathrm{q}}) \in [0, 1]$ if j is vaccinated. Otherwise, the individual becomes infectious with mild symptoms ($X_j(t^+) = \mathrm{I}$).

Recovery. An infected individual $j \in \mathcal{V}$ with $X_j(t^-) \in \{\mathrm{I}, \mathrm{Q}\}$ spontaneously recovers when a Poisson clock with a rate of $\beta \in \mathbb{R}_{>0}$ ticks, thereby returning to a susceptible health state ($X_j(t^+) = \mathrm{S}$).

Testing. The implementation of free testing campaigns induces mildly symptomatic infectious individuals to get tested. To model the effect of free testing, we employ a Poisson clock with a rate of $\tau \in \mathbb{R}_{\geq 0}$, representing the testing rate. Hence, an infectious individual j with mild symptoms ($X_j(t^-) = \mathrm{I}$) receives a diagnosis when a Poisson clock with a rate of τ ticks. After being diagnosed, j goes in quarantine ($X_j(t^+) = \mathrm{Q}$) and maintains physical distance from other individuals until recovery takes place. Here, we assume perfect testing, but further testing features such as false negatives could readily be incorporated by adding extra probabilistic mechanisms (e.g., see [34]).

Table 1 presents a summary of all the parameters. Note that all parameters with a domain in $[0, 1]$ or $[0, 1)$ are interpreted as probabilities.

Before presenting the analysis of the dynamics and our main theoretical results, we would like to comment that our

modeling framework is adaptable to several extensions and generalizations toward even more realistic settings.

Remark 1. *Our model fits the implementation of non-pharmaceutical interventions by introducing a parameter $\eta \in [0,1]$ that captures their effectiveness in reducing the per-contact infection probability, similar to [1], [18]. By replacing all the occurrences of λ with $(1-\eta)\lambda$, we effortlessly extend all our analytical findings to this scenario.*

Remark 2. *Without changing the fabric of our modeling framework, we can capture further features of epidemic diseases by incorporating additional health states and transitions. For instance, we may capture temporary or permanent natural immunity after recovery by adding a health state and extending our SIQS model to a SIQR(S) model, which has been proven effective in modeling the COVID-19 spread [19], [20], [35]. Furthermore, one can introduce heterogeneity in the recovery rate to represent, e.g., the effect of a vaccine in reducing the illness duration.*

Remark 3. *Although we assumed it to be constant here, the responsibility level of any individual $j \in \mathcal{V}$, σ_j, may be time-varying in general, influenced by co-evolving opinion formation processes and the epidemic spreading. To model such a temporal evolution, one could directly incorporate opinion dynamics [36], [37] or game-theoretic update mechanisms [38], [39], [40], [41] within the modeling framework.*

While the extension in Remark 1 is straightforward, the others may complicate or hinder the analytical tractability of the system. For this reason, we will perform the theoretical analysis of the original implementation of the SIQS model in the following sections, which one could interpret as a worst-case scenario for a model with natural immunity (such as a SIQR(S) model). Subsequently, we will embark on a case study in Section 5, employing numerical simulations to investigate the generalization discussed in Remark 2.

3.4 Dynamics

All the mechanisms described in Section 3.3 are induced by independent Poisson clocks, which implies that the evolution of the n-dimensional state

$$X(t) := [X_1(t), X_2(t), \dots, X_n(t)] \in \{\mathrm{S}, \mathrm{I}, \mathrm{Q}\}^n$$

is governed by a continuous-time Markov process [31].

Each individual can experience five distinct state transitions (illustrated in the diagram in Fig. 1), triggered by the processes of contagion, recovery, and testing. The two transitions triggered by recovery (from I and Q to S) and the one triggered by testing (from I to Q) solely involve spontaneous mechanisms. Hence, these three transition rates simply amount to the rates of the corresponding Poisson processes that trigger them. On the contrary, the two transitions induced by contagion (from S to I and Q) are related to the individual's vaccination status, interactions between individuals, and the health states of the others. Hence, they have a more intricate time-varying expression, as is shown in Proposition 3. For the sake of readability, we omit to stress that the rates and the health states of individuals are functions of time.

Proposition 3. *A non-vaccinated individual j with $X_j(t^-) = \mathrm{S}$ becomes infectious ($X_j(t^+) = \mathrm{I}$) according to a Poisson clock with a rate of*

$$\kappa_{\mathrm{n},j} := 2\lambda\,(1-p_{\mathrm{q}}) \cdot \left[\tfrac{\theta}{n(1-v)-1} \sum_{k\in\mathcal{V}_{\mathrm{n}}:X_k=\mathrm{I}} (1-\sigma_k) + \tfrac{1-\theta}{n-1} \sum_{k\in\mathcal{V}:X_k=\mathrm{I}} (1-\sigma_k)\right], \tag{2}$$

while they become quarantined ($X_j(t^+) = \mathrm{Q}$) with a rate of

$$\nu_{\mathrm{n},j} := 2\lambda p_{\mathrm{q}} \cdot \left[\tfrac{\theta}{n(1-v)-1} \sum_{k\in\mathcal{V}_{\mathrm{n}}:X_k=\mathrm{I}} (1-\sigma_k) + \tfrac{1-\theta}{n-1} \sum_{k\in\mathcal{V}:X_k=\mathrm{I}} (1-\sigma_k)\right], \tag{3}$$

A susceptible vaccinated individual j ($X_j(t^-) = \mathrm{S}$) becomes infectious ($X_j(t^+) = \mathrm{I}$) according to a Poisson clock with a rate of

$$\kappa_{\mathrm{v},j} := 2\lambda(1-\gamma_{\mathrm{t}})\big(1-p_{\mathrm{q}}(1-\gamma_{\mathrm{q}})\big) \cdot \left[\tfrac{1-\theta}{n-1} \sum_{k\in\mathcal{V}:X_k=\mathrm{I}} (1-\sigma_k) + \tfrac{\theta}{nv-1} \sum_{k\in\mathcal{V}_{\mathrm{v}}:X_k=\mathrm{I}} (1-\sigma_k)\right], \tag{4}$$

while they become quarantined ($X_j(t^+) = \mathrm{Q}$) with a rate of

$$\nu_{\mathrm{v},j} := 2\lambda(1-\gamma_{\mathrm{t}})p_{\mathrm{q}}(1-\gamma_{\mathrm{q}}) \cdot \left[\tfrac{1-\theta}{n-1} \sum_{k\in\mathcal{V}:X_k=\mathrm{I}} (1-\sigma_k) + \tfrac{\theta}{nv-1} \sum_{k\in\mathcal{V}_{\mathrm{v}}:X_k=\mathrm{I}} (1-\sigma_k)\right]. \tag{5}$$

Proof. Let us focus on the transition rates of a susceptible, non-vaccinated individual j. These transitions occur due to moments of contact between j and an infectious individual, which take place if one of the following mutually exclusive events happens: i) j activates, decides to interact only within its subpopulation, selects an infected individual in $\mathcal{V}_{\mathrm{n}}$, and the latter decides to have contact (i.e., to disregard physical distance); ii) an infected individual in $\mathcal{V}_{\mathrm{n}}$ activates, interacts only within its subpopulation, selects j, and the former decides to have contact; iii) j activates, interacts disregarding the subpopulation structure with an infected individual in $\mathcal{V}$, who decides to have contact; iv) an infected individual in $\mathcal{V}$ activates, interacts disregarding the subpopulation structure with j, and the former decides to have contact.

We observe that i) takes place if three independent events occur: E_1, the activation of j, which is triggered by a unit rate Poisson clock; E_2, the decision to interact only in the community, which occurs with probability $\mathbb{P}[E_2] = \theta$; and E_3, the selection of an infected individual $k \in \mathcal{V}_{\mathrm{n}}$ who decides to have close contact, which occurs with probability

$$\mathbb{P}[E_3] = \frac{1}{n(1-v)-1} \sum\nolimits_{k\in\mathcal{V}_{\mathrm{n}}:X_k=\mathrm{I}} (1-\sigma_k). \tag{6}$$

The flow splitting property in Proposition 2 allows us to compute the total rate associated with event i) as the product between the rate of event E_1 and the splitting probabilities $\mathbb{P}[E_2]$ and $\mathbb{P}[E_3]$. Similarly, we compute the rate associated with ii), iii), and iv). Next, we apply the flow aggregation property in Proposition 1 to find the rate related to the occurrence of contact between j and an infected individual; that is, by summing the rates corresponding to the four mutually exclusive events i)–iv), we obtain the rate

$$\chi := \tfrac{2\theta}{n(1-v)-1} \sum_{k\in\mathcal{V}:X_k=\mathrm{I}} (1-\sigma_k) + 2\tfrac{1-\theta}{n-1} \sum_{k\in\mathcal{V}_{\mathrm{v}}:X_k=\mathrm{I}} (1-\sigma_k). \tag{7}$$

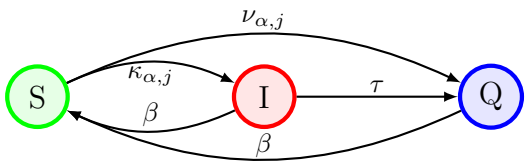

Fig. 1: State transitions of the epidemic model for an individual $j \in \mathcal{V}_\alpha$ with a vaccination status $\alpha \in \{\mathrm{n}, \mathrm{v}\}$.

Finally, note that a non-vaccinated individual j becomes infectious (I) after contact with an infected individual with probability $\lambda(1-p_\mathrm{q})$, while j becomes quarantined (Q) with probability λp_q. By the flow splitting property in Proposition 2, we obtain (2) and (3). Likewise, we derive (4) and (5) for a susceptible vaccinated individual. □

For a generic individual $j \in \mathcal{V}$, the transition rate matrix of the Markov process $X_j(t)$ is given by

$$Q_{\alpha,j} = \begin{bmatrix} -\kappa_{\alpha,j} - \nu_{\alpha,j} & \kappa_{\alpha,j} & \nu_{\alpha,j} \\ \beta & -\beta-\tau & \tau \\ \beta & 0 & -\beta \end{bmatrix}, \tag{8}$$

where $\alpha \in \{\mathrm{n}, \mathrm{v}\}$ is the vaccination status of j, and the rows (columns) correspond to states S, I, and Q, respectively.

The first row of (8) depends on the states of the other population members, making it impossible to decouple the individual dynamics. For a large-scale population, this impedes the analysis, as the dimension of the state space $X(t)$ increases exponentially with n. Hence, as is standard practice [28], we employ a mean-field approach, which will be key to deriving analytical results. Rather than studying how the health state of an individual $j \in \mathcal{V}$ evolves, we study the evolution of the probability that j is in a particular health state, where there is a probability assigned to every health state. Specifically, for any vaccination status $\alpha \in \{\mathrm{n}, \mathrm{v}\}$ and individual $j \in \mathcal{V}$, we define the probability that j is susceptible, infectious, or quarantined as

$$\begin{aligned} s_{\alpha,j}(t) &:= \mathbb{P}\left[X_j(t) = \mathrm{S}, j \in \mathcal{V}_\alpha\right], \\ i_{\alpha,j}(t) &:= \mathbb{P}\left[X_j(t) = \mathrm{I}, j \in \mathcal{V}_\alpha\right], \\ q_{\alpha,j}(t) &:= \mathbb{P}\left[X_j(t) = \mathrm{Q}, j \in \mathcal{V}_\alpha\right], \end{aligned} \tag{9}$$

respectively, where $s_{\mathrm{v},j}(t) = i_{\mathrm{v},j}(t) = q_{\mathrm{v},j}(t) = 0$ if $j \in \mathcal{V}_\mathrm{n}$, and $s_{\mathrm{n},j}(t) = i_{\mathrm{n},j}(t) = q_{\mathrm{n},j}(t) = 0$ if $j \in \mathcal{V}_\mathrm{v}$.

4 Analysis and Main Results

In this section, we present our main theoretical results. To reduce the number of parameters, we now assume a homogeneous responsibility level within a subpopulation, as summarized in Assumption 1.

Assumption 1. *Let $\sigma_i = \sigma_\mathrm{v} \in [0,1]$ for all $i \in \mathcal{V}_\mathrm{v}$, and $\sigma_j = \sigma_\mathrm{n} \in [0,1]$ for all $j \in \mathcal{V}_\mathrm{n}$, which denote the responsibility level of vaccinated and non-vaccinated individuals, respectively.*

4.1 Mean-field dynamics

By taking a mean-field approach, we study the evolution of the probabilities in (9). Their evolution is approximated by their expected dynamics [28], [29], i.e.,

$$\begin{aligned} (\dot{s}_{\mathrm{v},j}\ \dot{i}_{\mathrm{v},j}\ \dot{q}_{\mathrm{v},j}) &= (s_{\mathrm{v},j}\ i_{\mathrm{v},j}\ q_{\mathrm{v},j})\mathbb{E}[Q_{\mathrm{v},j}], \\ (\dot{s}_{\mathrm{n},j}\ \dot{i}_{\mathrm{n},j}\ \dot{q}_{\mathrm{n},j}) &= (s_{\mathrm{n},j}\ i_{\mathrm{n},j}\ q_{\mathrm{n},j})\mathbb{E}[Q_{\mathrm{n},j}], \end{aligned} \tag{10}$$

which yields the following dynamical system.

Proposition 4. *Let Assumption 1 hold. In the mean-field approximation,* (9) *follows*

$$\begin{aligned} \dot{s}_{\mathrm{n},j} &= -\lambda\bar{\alpha}_{\mathrm{n},j}s_{\mathrm{n},j} + \beta i_{\mathrm{n},j} + \beta q_{\mathrm{n},j}, \\ \dot{i}_{\mathrm{n},j} &= (1-p_\mathrm{q})\lambda\bar{\alpha}_{\mathrm{n},j}s_{\mathrm{n},j} - (\beta+\tau)i_{\mathrm{n},j}, \\ \dot{q}_{\mathrm{n},j} &= p_\mathrm{q}\lambda\bar{\alpha}_{\mathrm{n},j}s_{\mathrm{n},j} + \tau i_{\mathrm{n},j} - \beta q_{\mathrm{n},j}, \\ \dot{s}_{\mathrm{v},j} &= -\lambda\left(1-\gamma_\mathrm{t}\right)\bar{\alpha}_{\mathrm{v},j}s_{\mathrm{v},j} + \beta i_{\mathrm{v},j} + \beta q_{\mathrm{v},j}, \\ \dot{i}_{\mathrm{v},j} &= \left[1-p_\mathrm{q}\left(1-\gamma_\mathrm{q}\right)\right]\lambda\left(1-\gamma_\mathrm{t}\right)\bar{\alpha}_{\mathrm{v},j}s_{\mathrm{v},j} - (\beta+\tau)i_{\mathrm{v},j}, \\ \dot{q}_{\mathrm{v},j} &= p_\mathrm{q}\left(1-\gamma_\mathrm{q}\right)\lambda\left(1-\gamma_\mathrm{t}\right)\bar{\alpha}_{\mathrm{v},j}s_{\mathrm{v},j} + \tau i_{\mathrm{v},j} - \beta q_{\mathrm{v},j}, \end{aligned} \tag{11}$$

for all $j \in \mathcal{V}$, where

$$\begin{aligned} \bar{\alpha}_{\mathrm{n},j} :=& 2(1-\sigma_\mathrm{n})\left[\frac{\theta}{n(1-v)-1} + \frac{1-\theta}{n-1}\right]\sum_{k\in\mathcal{V}\setminus\{j\}} i_{\mathrm{n},k} \\ &+ 2(1-\sigma_\mathrm{v})\frac{1-\theta}{n-1}\sum_{k\in\mathcal{V}\setminus\{j\}} i_{\mathrm{v},k}, \end{aligned} \tag{12}$$

$$\begin{aligned} \bar{\alpha}_{\mathrm{v},j} :=& 2(1-\sigma_\mathrm{n})\frac{1-\theta}{n-1}\sum_{k\in\mathcal{V}\setminus\{j\}} i_{\mathrm{n},k} \\ &+ 2(1-\sigma_\mathrm{v})\left[\frac{\theta}{nv-1} + \frac{1-\theta}{n-1}\right]\sum_{k\in\mathcal{V}\setminus\{j\}} i_{\mathrm{v},k}. \end{aligned} \tag{13}$$

Proof. First, we observe that the transition rates in Proposition 3 simplify under Assumption 1, as we can collect all the similar terms in the summations and obtain, e.g.,

$$\begin{aligned} \kappa_{\mathrm{n},j} = 2\lambda\left(1-p_\mathrm{q}\right)\Bigg[&(1-\sigma_\mathrm{v})\tfrac{1-\theta}{n-1}\textstyle\sum_{k\in\mathcal{V}_\mathrm{v}:X_k=\mathrm{I}} 1 \\ &+ (1-\sigma_\mathrm{n})\left(\tfrac{\theta}{n(1-v)-1} + \tfrac{1-\theta}{n-1}\right)\textstyle\sum_{k\in\mathcal{V}_\mathrm{n}:X_k=\mathrm{I}} 1\Bigg]. \end{aligned} \tag{14}$$

The same holds for the rates in Eqs. (3)–(5). Next, when computing the entries $\mathbb{E}[\kappa_{\alpha,j}]$ and $\mathbb{E}[\nu_{\alpha,j}]$ of $\mathbb{E}[Q_{\alpha,j}]$, note that for any susceptible individual $j \in \mathcal{V}$ ($X_j(t) = \mathrm{S}$) it holds that

$$\mathbb{E}\left[\sum_{k\in\mathcal{V}_\alpha:X_k=\mathrm{I}} 1\right] = \sum_{k\in\mathcal{V}\setminus\{j\}} i_{\alpha,k}, \tag{15}$$

for a vaccination status $\alpha \in \{\mathrm{n}, \mathrm{v}\}$. Substituting (15) into the expected dynamics yields the rest of the proof. □

From Proposition 4, we observe that the mean-field dynamics are nontrivial. In particular, the system in Eq. (11) has two nonlinear terms accounting for the contagion probability if j is susceptible: i) $\lambda\bar{\alpha}_{\mathrm{n},j}$ if j if non-vaccinated and ii) $\lambda(1-\gamma_\mathrm{t})\bar{\alpha}_{\mathrm{v},j}$ if j is vaccinated. These two nonlinear terms couple the evolution of individual j with all other individuals through the expressions in Eqs. (12)–(13).

We will now show that the system in (11) is well-defined by showing that $(s_{\mathrm{n},j}\ i_{\mathrm{n},j}\ q_{\mathrm{n},j}\ s_{\mathrm{v},j}\ i_{\mathrm{v},j}\ q_{\mathrm{v},j})$ is a probability vector for all $t \in \mathbb{R}_{\geq 0}$ and $j \in \mathcal{V}$. For this purpose, let us define the following sets. For any $j \in \mathcal{V}_\mathrm{n}$, we have

$$\mathcal{S}_{\mathrm{n},j} := \left\{(s_{\mathrm{n},j}\ i_{\mathrm{n},j}\ q_{\mathrm{n},j}\ s_{\mathrm{v},j}\ i_{\mathrm{v},j}\ q_{\mathrm{v},j}) \;\middle|\; \begin{array}{l} s_{\mathrm{n},j}, i_{\mathrm{n},j}, q_{\mathrm{n},j} \geq 0, \\ s_{\mathrm{v},j} = i_{\mathrm{v},j} = q_{\mathrm{v},j} = 0, \\ s_{\mathrm{n},j} + i_{\mathrm{n},j} + q_{\mathrm{n},j} = 1 \end{array}\right\},$$

while for any $j \in \mathcal{V}_\mathrm{v}$, we have

$$\mathcal{S}_{\mathrm{v},j} := \left\{(s_{\mathrm{n},j}\ i_{\mathrm{n},j}\ q_{\mathrm{n},j}\ s_{\mathrm{v},j}\ i_{\mathrm{v},j}\ q_{\mathrm{v},j}) \;\middle|\; \begin{array}{l} s_{\mathrm{n},j} = i_{\mathrm{n},j} = q_{\mathrm{n},j} = 0, \\ s_{\mathrm{v},j}, i_{\mathrm{v},j}, q_{\mathrm{v},j} \geq 0, \\ s_{\mathrm{v},j} + i_{\mathrm{v},j} + q_{\mathrm{v},j} = 1 \end{array}\right\}.$$

Lemma 1. *For all $j \in \mathcal{V}_{\mathrm{n}}$, the set $\mathcal{S}_{\mathrm{n},j}$ is positive invariant under* (11). *Likewise, $\mathcal{S}_{\mathrm{v},j}$ is positive invariant for all $j \in \mathcal{V}_{\mathrm{v}}$.*

Proof. Let us consider $\mathcal{S}_{\mathrm{n},j}$ for any $j \in \mathcal{V}_{\mathrm{n}}$. First, note that if one of the probabilities governed by (11) equals zero, then its respective time-derivative is non-negative. Next, observe that $s_{\mathrm{v},j} = i_{\mathrm{v},j} = q_{\mathrm{v},j} = 0$ implies that the time-derivatives of $s_{\mathrm{v},j}$, $i_{\mathrm{v},j}$, and $q_{\mathrm{v},j}$ are zero. Now note that for all $j \in \mathcal{V}_{\mathrm{n}}$, $\dot{s}_{\mathrm{n},j} + \dot{i}_{\mathrm{n},j} + \dot{q}_{\mathrm{n},j} = 0$, so $s_{\mathrm{n},j} + i_{\mathrm{n},j} + q_{\mathrm{n},j} = 1$ for all $t \in \mathbb{R}_{\geq 0}$. The proof works analogously for $\mathcal{S}_{\mathrm{v},j}$. □

To commence the mean-field analysis of the system, let us denote the average probability for a randomly selected individual to have vaccination status $\alpha \in \{\mathrm{n}, \mathrm{v}\}$ and be susceptible, infectious, or quarantined as

$$y_{\alpha,\mathrm{s}} := \frac{1}{n}\sum_{j\in\mathcal{V}} s_{\alpha,j}, \quad y_{\alpha,\mathrm{i}} := \frac{1}{n}\sum_{j\in\mathcal{V}} i_{\alpha,j}, \quad y_{\alpha,\mathrm{q}} := \frac{1}{n}\sum_{j\in\mathcal{V}} q_{\alpha,j}, \tag{16}$$

respectively.

By taking a sufficiently large population size n, the fraction of individuals in a state can be arbitrarily closely approximated by the average probability to be in that state, for any finite time-horizon [32], [42]—that is, for an $\alpha \in \{\mathrm{n}, \mathrm{v}\}$,

$$\begin{aligned} S_\alpha(t) &:= \tfrac{1}{n}|\{j \in \mathcal{V}_\alpha : X_j(t) = \mathrm{S}\}| \approx y_{\alpha,\mathrm{s}}, \\ I_\alpha(t) &:= \tfrac{1}{n}|\{j \in \mathcal{V}_\alpha : X_j(t) = \mathrm{I}\}| \approx y_{\alpha,\mathrm{i}}, \\ Q_\alpha(t) &:= \tfrac{1}{n}|\{j \in \mathcal{V}_\alpha : X_j(t) = \mathrm{Q}\}| \approx y_{\alpha,\mathrm{q}}, \end{aligned} \tag{17}$$

as illustrated in Fig. 2.

Since the average probabilities in (16) adequately reflect the state of a sufficiently large population, we now focus on the dynamics of the macroscopic variables in (16), presented in the following proposition.

Proposition 5. *Consider the system in* (11). *In the thermodynamic limit of large-scale systems $n \to \infty$, the dynamics of* (16) *are given by*

$$\begin{aligned} \dot{y}_{\mathrm{n,s}} =& -2\lambda\Big(\tfrac{\theta}{1-v} + 1 - \theta\Big)(1-\sigma_{\mathrm{n}})y_{\mathrm{n,s}}y_{\mathrm{n,i}} \\ & - 2\lambda(1-\theta)(1-\sigma_{\mathrm{v}})y_{\mathrm{n,s}}y_{\mathrm{v,i}} + \beta y_{\mathrm{n,i}} + \beta y_{\mathrm{n,q}}\,, \\ \dot{y}_{\mathrm{n,i}} =& 2\lambda(1-p_{\mathrm{q}})\Big(\tfrac{\theta}{1-v} + 1 - \theta\Big)(1-\sigma_{\mathrm{n}})y_{\mathrm{n,s}}y_{\mathrm{n,i}} \\ & + 2\lambda(1-p_{\mathrm{q}})(1-\theta)(1-\sigma_{\mathrm{v}})y_{\mathrm{n,s}}y_{\mathrm{v,i}} - (\beta+\tau)y_{\mathrm{n,i}}\,, \\ \dot{y}_{\mathrm{n,q}} =& 2\lambda p_{\mathrm{q}}\Big(\tfrac{\theta}{1-v} + 1 - \theta\Big)(1-\sigma_{\mathrm{n}})y_{\mathrm{n,s}}y_{\mathrm{n,i}} \\ & + 2\lambda p_{\mathrm{q}}(1-\theta)(1-\sigma_{\mathrm{v}})y_{\mathrm{n,s}}y_{\mathrm{v,i}} + \tau y_{\mathrm{n,i}} - \beta y_{\mathrm{n,q}}\,, \\ \dot{y}_{\mathrm{v,s}} =& -2\lambda(1-\gamma_{\mathrm{t}})(1-\theta)(1-\sigma_{\mathrm{n}})y_{\mathrm{v,s}}y_{\mathrm{n,i}} + \beta y_{\mathrm{v,i}} \\ & - 2\lambda(1-\gamma_{\mathrm{t}})\Big(\tfrac{\theta}{v} + 1 - \theta\Big)(1-\sigma_{\mathrm{v}})y_{\mathrm{v,s}}y_{\mathrm{v,i}} + \beta y_{\mathrm{v,q}}\,, \\ \dot{y}_{\mathrm{v,i}} =& 2\lambda(1-\gamma_{\mathrm{t}})[1-p_{\mathrm{q}}(1-\gamma_{\mathrm{q}})](1-\theta)(1-\sigma_{\mathrm{n}})y_{\mathrm{v,s}}y_{\mathrm{n,i}} \\ & + 2\lambda(1-\gamma_{\mathrm{t}})[1-p_{\mathrm{q}}(1-\gamma_{\mathrm{q}})] \\ & \cdot \Big(\tfrac{\theta}{v} + 1 - \theta\Big)(1-\sigma_{\mathrm{v}})y_{\mathrm{v,s}}y_{\mathrm{v,i}} - (\beta+\tau)y_{\mathrm{v,i}}\,, \\ \dot{y}_{\mathrm{v,q}} =& 2\lambda(1-\gamma_{\mathrm{t}})p_{\mathrm{q}}(1-\gamma_{\mathrm{q}})(1-\theta)(1-\sigma_{\mathrm{n}})y_{\mathrm{v,s}}y_{\mathrm{n,i}} \\ & + 2\lambda(1-\gamma_{\mathrm{t}})p_{\mathrm{q}}(1-\gamma_{\mathrm{q}})\Big(\tfrac{\theta}{v} + 1 - \theta\Big)(1-\sigma_{\mathrm{v}})y_{\mathrm{v,s}}y_{\mathrm{v,i}} \\ & + \tau y_{\mathrm{v,i}} - \beta y_{\mathrm{v,q}}\,. \end{aligned} \tag{18}$$

Proof. Computing the temporal derivatives of the expressions in (16) while using Proposition 4 gives the system presented in (18). □

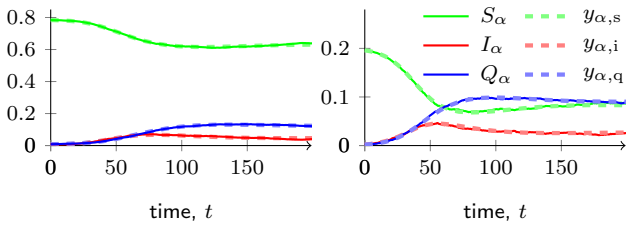

(a) $\alpha = \mathrm{v}$ (b) $\alpha = \mathrm{n}$

Fig. 2: Comparison of the quantities in (17) via a simulation of the Markov process (solid) and its deterministic approximation from Proposition 5 (dashed). Parameters are $n = 20\,000$, $v = 0.8$, $\lambda = 0.2$, $\sigma_{\mathrm{v}} = 0.7$, $\sigma_{\mathrm{n}} = 0.2$, $p_{\mathrm{q}} = 0.2$, $\beta = 0.02$, $\gamma_{\mathrm{t}} = 0.5$, $\gamma_{\mathrm{q}} = 0.9$, $\tau = 0.05$, and $\theta = 0.5$.

Remark 4. *Only 4 of the 6 equations in* (18) *are linearly independent since $y_{\mathrm{v,s}} + y_{\mathrm{v,i}} + y_{\mathrm{v,q}} = v$ and $y_{\mathrm{n,s}} + y_{\mathrm{n,i}} + y_{\mathrm{n,q}} = 1 - v$.*

4.2 Epidemic threshold

Here, we study whether a local infection outbreak leads to endemicity in the population. Theorem 1 presents the conditions for the *epidemic threshold*, which is formulated as the testing rate $\bar{\tau}$ above which the disease-free equilibrium (DFE) of (18) (with $y_{\mathrm{n,i}} = y_{\mathrm{n,q}} = y_{\mathrm{v,i}} = y_{\mathrm{v,q}} = 0$) is locally asymptotically stable. If the testing rate τ exceeds the threshold $\bar{\tau}$, then the local outbreak will be eradicated. If not, it will lead to endemicity. The proof is reported in Appendix A.

Theorem 1. *Consider the system in* (18). *The epidemic threshold is equal to*

$$\bar{\tau} := \lambda\xi - \beta + \lambda\sqrt{\xi^2 - 4\theta(1-\gamma_{\mathrm{t}})(1-p_{\mathrm{q}})[1-p_{\mathrm{q}}(1-\gamma_{\mathrm{q}})](1-\sigma_{\mathrm{n}})(1-\sigma_{\mathrm{v}})}, \tag{19}$$

where

$$\begin{aligned} \xi :=& (1-p_{\mathrm{q}})(1-\sigma_{\mathrm{n}})[\theta + (1-\theta)(1-v)] \\ & + (1-\gamma_{\mathrm{t}})[1-p_{\mathrm{q}}(1-\gamma_{\mathrm{q}})](1-\sigma_{\mathrm{v}})[\theta + (1-\theta)v]. \end{aligned} \tag{20}$$

If $\tau > \bar{\tau}$, the DFE is locally asymptotically stable.

Remark 5. *Observe from* (19) *that if the recovery rate satisfies*

$$\beta > \lambda\xi + \lambda\sqrt{\xi^2 - 4\theta(1-\gamma_{\mathrm{t}})(1-p_{\mathrm{q}})[1-p_{\mathrm{q}}(1-\gamma_{\mathrm{q}})](1-\sigma_{\mathrm{n}})(1-\sigma_{\mathrm{v}})}, \tag{21}$$

then no control is needed, since the DFE is always locally asymptotically stable.

Corollary 1. *In the absence of homophily—i.e., if $\theta = 0$ and the multi-population structure does not influence individuals' interactions—the epidemic threshold in* (19) *reduces to*

$$\begin{aligned} \tau^* :=& 2\lambda(1-\sigma_{\mathrm{n}})(1-v)(1-p_{\mathrm{q}}) \\ & + 2\lambda v(1-\sigma_{\mathrm{v}})(1-\gamma_{\mathrm{t}})[1-p_{\mathrm{q}}(1-\gamma_{\mathrm{q}})] - \beta. \end{aligned} \tag{22}$$

Although the expression of the epidemic threshold in Theorem 1 is generally intricate, we can immediately observe the monotonicity properties in the following proposition. These properties are derived directly from the stability analysis of the DFE, as reported in Appendix B.

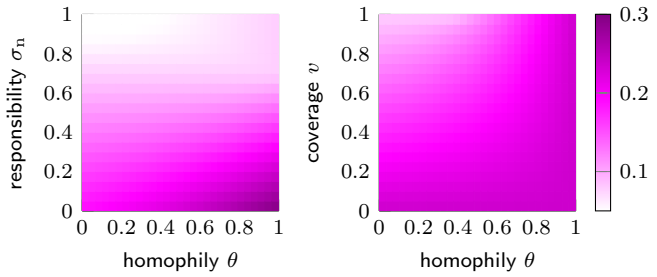

(a) $v = 0.5$ (b) $\sigma_n = 0.2$

Fig. 3: The epidemic threshold $\bar{\tau}$ (color-coded) computed using (19) for different values of the model parameters. Common parameters are $\lambda = 0.2$, $\sigma_v = 0.5$, $p_q = 0.2$, $\beta = 0.02$, $\gamma_t = 0.5$, $\gamma_q = 0.9$, and $\tau = 0.05$.

Proposition 6. *An increase in the infection probability λ or the effectiveness of the vaccine against severe illness γ_q leads to an increase in the epidemic threshold $\bar{\tau}$ in* (19)*. Contrarily, $\bar{\tau}$ decreases with increases in the recovery rate β, the effectiveness of the vaccine against transmission γ_t, the responsibilities σ_v and σ_n, and the probability of developing severe illness p_q.*

Proposition 6 states that while an increase in a vaccine's effectiveness against transmission generally facilitates the eradication of an epidemic outbreak, its effectiveness against severe illness raises the threshold, hindering the controllability of the disease. This phenomenon may arise as infected individuals with non-severe symptoms go undetected, thereby fueling disease transmission, which may help explain the epidemic outbreaks that transpired after the COVID-19 vaccination campaign.

The impact of the remaining parameters (the vaccination coverage v and the homophily θ) is less intuitive, however. Of particular interest is understanding the role of vaccination coverage in facilitating or deterring epidemic outbreaks. To shed light on this matter, we perform a sensitivity analysis of the threshold in (19), summarized in the following proposition.

Proposition 7. *An increase in the vaccination coverage v decreases the epidemic threshold $\bar{\tau}$ in* (19) *if and only if*

$$(1-\gamma_t)(1-p_q(1-\gamma_q))(1-\sigma_v)-(1-p_q)(1-\sigma_n) < 0. \quad (23)$$

Proof. The condition in (23) is obtained by computing the partial derivative of $\bar{\tau}$ with respect to v, which is equal to the left-hand side of (23) multiplied by a positive quantity. □

From Proposition 7, we observe that the level of vaccination coverage has an ambiguous effect on the epidemic threshold. In particular, whether an increase in vaccination coverage facilitates the prevention of an epidemic outbreak depends on the characteristics of the vaccine (i.e., its effectiveness against transmission and severe illness), the probability of developing severe illness, and the responsibility of vaccinated and non-vaccinated individuals. This is consistent with the observations made on a simpler model in [1].

Finally, Figure 3 reports some observations concerning the role of the homophily level θ. Our numerical simulations show that high levels of homophily facilitate the spread of epidemic diseases, particularly when combined with lower levels of responsibility for non-vaccinated individuals. This suggests that neglecting the polarization that can emerge during a pandemic—with clusters of individuals who disregard the use of protective measures and refuse to be vaccinated—may lead to a dangerous underestimation of the risk of a local outbreak.

4.3 Endemic equilibrium

To conclude this section, we observe that while vaccination may exhibit a complex and unexpected effect on epidemic outbreak control, calling for an increased testing effort, its impact on mitigating endemic prevalence is more predictable. In fact, the simulations reported in Fig. 4 suggest that increasing the vaccination coverage of a population is always beneficial—the number of infections decreases if the vaccination coverage v increases—excluding the specific scenario in which non-vaccinated individuals are significantly more responsible than their vaccinated peers. In this scenario, increasing the vaccination coverage may be harmful, as illustrated in Fig. 4d.

Further insights can be gained by analyzing the behavior of (18) above the epidemic threshold (i.e., when the DFE is not locally asymptotically stable), but the high number of nonlinear terms in (18) hinders the system analysis above the threshold. Therefore, we will now focus on a specific scenario for which analytical results can be established.

Assumption 2. *Let $\sigma_v = 1$ and $\sigma_n < 1$.*

Under Assumption 2, non-vaccinated individuals are less responsible than their vaccinated peers, who always act responsibly. From Theorem 1, we note the following.

Corollary 2. *Under Assumption 2, the epidemic threshold in* (19) *reduces to*

$$\hat{\tau} := 2\lambda(1-\sigma_n)(1-p_q)[\theta+(1-\theta)(1-v)]-\beta\,. \quad (24)$$

Next, we present the main result of this section that characterizes all the equilibria of the system and their local stability properties. The proof can be found in Appendix C.

Theorem 2. *Under Assumption 2, the system in* (18) *has at most two equilibria:*

i) the DFE $(1-v, 0, 0, v, 0, 0)$, which is locally asymptotically stable if $\tau \geq \hat{\tau}$ (with exponential stability if strict inequality holds), and a saddle point if $\tau < \hat{\tau}$;

ii) the EE $(y^*_{n,s}, y^*_{n,i}, y^*_{n,q}, y^*_{v,s}, y^*_{v,i}, y^*_{v,q})$, which exists if and only if $\tau < \hat{\tau}$, where

$$\begin{aligned}
y^*_{n,s} &:= \tfrac{(\beta+\tau)(1-v)}{2\lambda(1-\sigma_n)[\theta+(1-\theta)(1-v)](1-p_q)}\,,\\
y^*_{n,i} &:= \beta\kappa\,,\\
y^*_{n,q} &:= 1-v-\tfrac{(\beta+\tau)(1-v)}{2\lambda(1-\sigma_n)[\theta+(1-\theta)(1-v)](1-p_q)}-\beta\kappa\,,\\
y^*_{v,s} &:= \tfrac{v}{1+2\lambda\kappa(1-\sigma_n)(1-\gamma_t)(1-\theta)}\,,\\
y^*_{v,i} &:= \tfrac{2\lambda\kappa v\beta(1-\sigma_n)(1-\gamma_t)(1-\theta)[1-p_q(1-\gamma_q)]}{(\beta+\tau)[1+2\lambda\kappa(1-\sigma_n)(1-\gamma_t)(1-\theta)]}\,,\\
y^*_{v,q} &:= \tfrac{2\lambda\kappa v(1-\sigma_n)(1-\gamma_t)(1-\theta)[\tau+p_q(1-\gamma_q)\beta]}{(\beta+\tau)[1+2\lambda\kappa(1-\sigma_n)(1-\gamma_t)(1-\theta)]}\,,
\end{aligned} \quad (25)$$

with

$$\kappa := (1-v)\left(\tfrac{1-p_q}{\beta+\tau}-\tfrac{1}{2\lambda(1-\sigma_n)[\theta+(1-\theta)(1-v)]}\right). \quad (26)$$

If it exists, the EE is locally asymptotically stable.

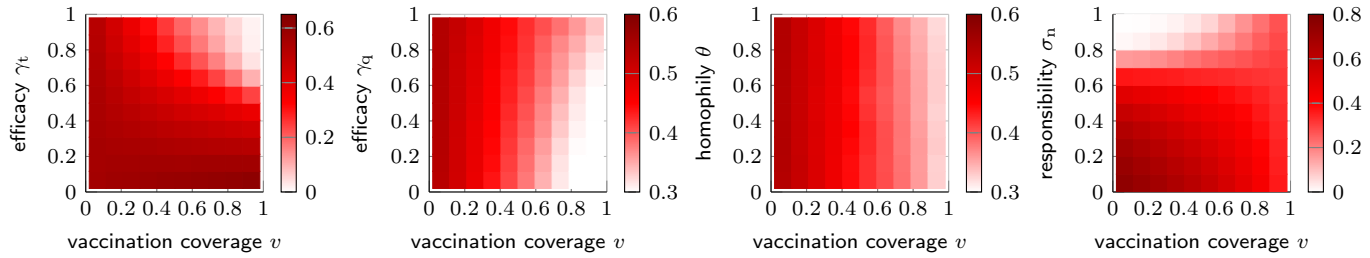

(a) $\sigma_n = \theta = 0.5, \gamma_q = 0.9$ (b) $\sigma_n = \theta = \gamma_t = 0.5$ (c) $\sigma_n = \gamma_t = 0.5, \gamma_q = 0.9$ (d) $\gamma_t = \theta = 0.5, \gamma_q = 0.9$

Fig. 4: Total fraction of infected individuals $I_v(t) + I_n(t) + Q_v(t) + Q_n(t)$ at $t = 200$ (color-coded) for different levels of the vaccination coverage v, with on the y-axis varying levels of: (a) the vaccine effectiveness against transmission γ_t and (b) severe symptoms γ_q; (c) the level of homophily θ; and (d) the responsibility of non-vaccinated individuals σ_n. Common parameter values are $n = 10\,000$, $\lambda = 0.2$, $\beta = 0.02$, $\sigma_v = 0.5$, $p_q = 0.2$, and $\tau = 0.05$. Each data-point is obtained by averaging 10 independent runs of the Markov process.

Despite the cumbersome expression of the EE in Theorem 2, we observe by computing the derivatives of $\frac{y^*_{n,s}}{1-v}$ and $\frac{y^*_{v,s}}{v}$ that an increase in the fraction of vaccinated individuals results in a decrease in the relative epidemic prevalence within both sub-populations. Such analytical insight confirms the numerical intuition from Fig. 4 that vaccination is always beneficial in reducing the epidemic prevalence, especially in the presence of a cluster of individuals with low responsibility, such as epidemic deniers [33]. Finally, one can use similar arguments to compute the EE for the opposite scenario with $\sigma_n = 1$ and $\sigma_v < 1$. Nonetheless, we omit to report such a result due to space constraints and its minor interest in the context of epidemic deniers, who typically refuse vaccination and responsible behaviors [43].

5 Numerical Results

In this section, we will expand on Remark 2 and employ numerical simulations while focusing on a case study motivated by the COVID-19 pandemic.

Earlier, in Remarks 1–3, we discussed how our modeling framework is open to several generalizations. For some of them, our analytical findings can be readily extended. For instance, as suggested in Remark 1, Theorem 1 can be expanded to incorporate non-pharmaceutical interventions by substituting λ with $(1-\eta)\lambda$ in (19), where $\eta \in [0,1]$ is the effectiveness of non-pharmaceutical interventions. Other extensions, however, increase the complexity of the dynamics, thereby hindering the analytical treatment and preventing a direct extension of the mean-field approach used to derive our theoretical findings. Nevertheless, the implementation of our model, grounded in the activity-driven network formalism, enables a numerical treatment via fast Monte Carlo simulation campaigns.

Following Remark 2, we expand our modeling framework by including an additional health state—denoted by R—to account for temporary immunity after recovery. We define this SIQRS model as an extension of our SIQS model, in which infected individuals (either in I or Q) transition to R when they recover and are (temporarily) immune to contagion. Loss of natural immunity is modeled through a Poisson process with a rate of $\mu \in \mathbb{R}_{\geq 0}$, where $\mu = 0$ represents the scenario in which immunity is permanent, and the limit $\mu \to \infty$ coincides with the SIQS model studied analytically in the above. A schematic of the SIQRS model is shown in Fig. 5.

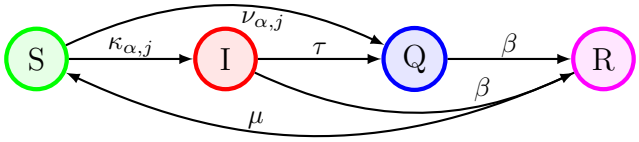

Fig. 5: State transitions of the SIQRS model for an individual $j \in \mathcal{V}_\alpha$ with a vaccination status $\alpha \in \{n, v\}$.

TABLE 2: Parameters of the COVID-19-inspired case study.

	n	λ	β	v	p_q	γ_t	γ_q
value	10 000	0.36	0.1	0.821	0.19	0.65	0.92

We consider a case study inspired by the ongoing COVID-19 pandemic and global vaccination campaign. Specifically, we utilize model parameters calibrated to reflect some characteristics of COVID-19 and the situation in the Netherlands as of early November 2021, estimated in our previous work [1] from clinical and epidemiological data [44], [45] and reported in Table 2. Considering the high level of uncertainty on the duration of natural immunity for COVID-19, which may strongly depend on the appearance of new variants [46], we will test different hypotheses on μ.

First, we perform a set of Monte Carlo simulations to show that the threshold behavior, proved analytically in Section 4 in the absence of natural immunity, is an inherent property of the epidemic model. To this aim, we numerically estimate the probability of disease eradication and the steady-state fraction of infected for different values of the testing rate τ and for four different natural immunity durations—spanning from an average of 1 week (which may represent the pessimistic scenario in which a new variant appears) to an average of 4 months.

Our simulations, reported in Fig. 6, confirm our analytical findings for the SIQS model in Section 4 (compare the gray curve and the gray dashed line in Fig. 6a). Furthermore, the simulations suggest that the threshold behavior is also an intrinsic property of the SIQRS model, although the duration of natural immunity affects the value of the

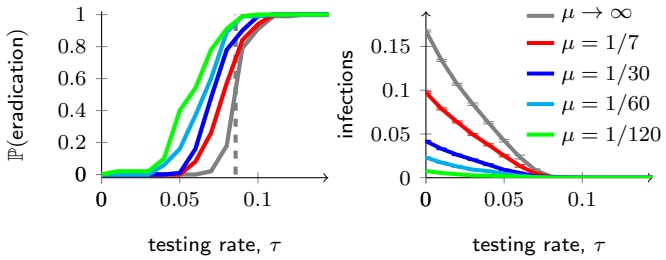

(a) Eradication probability (b) Steady-state fraction

Fig. 6: Numerical estimation for the SIQRS model (averaged over 100 independent runs) of (a) the eradication probability and (b) the steady-state fraction of infected individuals $I_{\mathrm{v}}(t) + I_{\mathrm{n}}(t) + Q_{\mathrm{v}}(t) + Q_{\mathrm{n}}(t)$ at $t = 200$, for increasing values of the control parameter τ and different duration of natural immunity μ. The gray curves and the gray vertical dashed line are, respectively, the numerical estimations and analytical computation of the threshold (using Theorem 1) for the SIQS model (which is equivalent to the SIQRS model in the limit $\mu \to \infty$). Common parameter values are $\sigma_{\mathrm{n}} = \theta = 0.5$ and $\sigma_{\mathrm{v}} = 0.7$; the rest of the parameter values are given in Table 2.

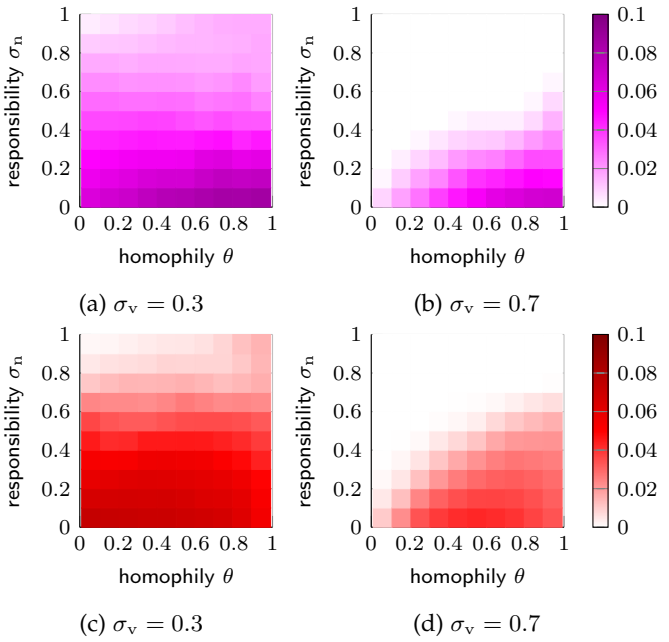

(a) $\sigma_{\mathrm{v}} = 0.3$ (b) $\sigma_{\mathrm{v}} = 0.7$

(c) $\sigma_{\mathrm{v}} = 0.3$ (d) $\sigma_{\mathrm{v}} = 0.7$

Fig. 7: (a,b) The epidemic threshold $\bar{\tau}$ (color-coded) estimated numerically for the COVID-inspired case study with a backbone network; and (c,d) the total fraction of infected individuals $I_{\mathrm{v}}(t) + I_{\mathrm{n}}(t) + Q_{\mathrm{v}}(t) + Q_{\mathrm{n}}(t)$ at $t = 200$ (color-coded), for different values of the model parameters. Common model parameter values are $\mu = 1/30$, $\tau = 0.02$, and those summarized in Table 2.

epidemic threshold, as illustrated in Fig. 6a. Predictably, the longer immunity lasts, the easier it is to control an epidemic outbreak. Moreover, when the testing rate τ is insufficient to reach disease eradication, the duration of natural immunity has a strong impact. In this scenario, an increase in the immunity duration leads to a decrease in the steady-state fraction of infected individuals, as reported in Figure 6b.

In light of these observations, we conduct a series of simulations to increase understanding of the impact of the model parameters on the progression of the epidemic. Here, we set $\mu = 1/30$. In Fig. 7, we report the epidemic threshold and the long-term fraction of infected individuals for different values of homophily θ and responsibility of non-vaccinated individuals σ_{n}. The threshold is estimated via a Monte Carlo-based approach detailed in Appendix D. Our simulation results in Fig. 7 suggest the following. First, individual responsibility is crucial: for low levels of responsibility, it is impossible to eradicate the disease without resorting to massive testing campaigns (Fig. 7c). Second, the role of homophily, already highlighted in our analytical results for the SIQS model, remains critical in the presence of natural immunity, in particular when vaccinated individuals have a higher responsibility level than non-vaccinated ones (Figs. 7b and 7d). This can, e.g., reflect the situation in which non-vaccinated individuals belong to a minority of conspiracy theorists, as COVID-19-related conspiracy belief has a negative correlation with the willingness to vaccinate and display infection-preventive behavior [43]. Third, the responsibility level of vaccinated individuals strongly impacts the epidemic threshold, but only if non-vaccinated people display some degree of responsible behavior and homophily is moderate, as can be observed by comparing the top-right of Figs. 7a and 7b. When above the threshold, we can observe by comparing Fig. 7c and Fig. 7d that the responsibility level of vaccinated individuals also plays a major role in reducing the fraction of infected individuals.

6 Conclusion

We proposed a polarized temporal multi-population network model to study the spread of recurrent epidemics and investigated the effect of vaccination campaigns, human behavior, and homophily on infection prevalence and local outbreak control. Via a mean-field approach, we analytically derived the epidemic threshold and, under certain assumptions, we characterized the endemic equilibrium. Additionally, we conducted numerical simulations on a generalization of our mathematical model that incorporates temporary natural immunity following recovery, utilizing parameters calibrated on the COVID-19 pandemic. Our results suggest that vaccination is a powerful measure to mitigate the number of deaths and the pressure on hospitals. However, the effectiveness of vaccination campaigns in controlling local outbreaks is contingent upon the characteristics of both the virus and the vaccine in question. In certain scenarios, relying solely on vaccination campaigns may have both beneficial and detrimental effects: while they alleviate the burden on healthcare systems, they may also impede the control of local outbreaks. Analytical and numerical findings suggest that, in these scenarios, complete disease eradication requires either reliance on population responsibility or widespread testing campaigns. Furthermore, our simulations showed that a polarized network structure with a high degree of homophily hinders local outbreak control.

Despite the generality of our modeling framework, some limitations should be noted. In particular, we assumed that individuals' decisions to vaccinate are fixed and made a priori. This assumption may be appropriate for certain

infections, such as influenza viruses, but it does not take into account situations in which vaccination decisions dynamically change. Moreover, our model operates under the assumption that individuals who support vaccination have already received the vaccine. To extend the model, one could consider incorporating changes in attitudes towards vaccination over time, as suggested in [47], [48], [49], and introducing vaccine administration during an epidemic outbreak, as in [18], [50].

In addition to incorporating these features in the model, there are several other directions for future research. Our numerical results for the SIQRS model suggest that the threshold phenomenon—proved analytically for the SIQS model—is an inherent feature of our epidemic framework. Future efforts should aim to extend our analytical results to models with extra compartments. Additionally, it would be useful to provide a more general analytical treatment of the system above the epidemic threshold. An expansion on Theorem 2 for more general conditions would be crucial for the development of optimal intervention policies, which could be achieved by incorporating a cost associated with the implementation of testing campaigns. Furthermore, for the sake of analytical tractability, we assumed that individuals' decisions on maintaining physical distance follow a memoryless mechanism. More realistic scenarios may include a game-theoretic decision-making process that accounts for individuals' past behaviors, societal pressure, the spread of the epidemic, and other external factors [38], [40], [41]. Finally, validating our framework against real-world data will be a priority in future research.

APPENDIX A
PROOF OF THEOREM 1

Observe that the disease-free equilibrium of (18) is the state

$$(y_{\mathrm{n,s}},\, y_{\mathrm{n,i}},\, y_{\mathrm{n,q}},\, y_{\mathrm{v,s}},\, y_{\mathrm{v,i}},\, y_{\mathrm{v,q}}) = (1-v, 0, 0, v, 0, 0),$$

which is an equilibrium since the right-hand side of (18) is equal to zero in this state. To study the local stability of the DFE, we recall that only four of the six equations of system (18) are linearly independent (Remark 4). In our analysis, we reduce the system to a 4-dimensional system by choosing the macroscopic variables $y_{\mathrm{n,i}}$, $y_{\mathrm{n,q}}$, $y_{\mathrm{v,i}}$, and $y_{\mathrm{v,q}}$. Subsequently, we linearize (18) around the DFE of the original system (which coincides with the origin of the reduced 4-dimensional one), yielding

$$\begin{aligned}
\dot{y}_{\mathrm{n,i}} =& 2\lambda(1-p_{\mathrm{q}})[\theta+(1-\theta)(1-v)](1-\sigma_{\mathrm{n}})y_{\mathrm{n,i}} \\
&+ 2\lambda(1-p_{\mathrm{q}})(1-\theta)(1-v)(1-\sigma_{\mathrm{v}})y_{\mathrm{v,i}} \\
&- (\beta+\tau)y_{\mathrm{n,i}}, \\
\dot{y}_{\mathrm{v,i}} =& 2\lambda(1-\gamma_{\mathrm{t}})[1-p_{\mathrm{q}}(1-\gamma_{\mathrm{q}})]v(1-\theta)(1-\sigma_{\mathrm{n}})y_{\mathrm{n,i}} \\
&+ 2\lambda(1-\gamma_{\mathrm{t}})[1-p_{\mathrm{q}}(1-\gamma_{\mathrm{q}})] \\
&\quad\cdot[\theta+v(1-\theta)](1-\sigma_{\mathrm{v}})y_{\mathrm{v,i}} - (\beta+\tau)y_{\mathrm{v,i}}, \\
\dot{y}_{\mathrm{n,q}} =& 2\lambda p_{\mathrm{q}}[\theta+(1-\theta)(1-v)](1-\sigma_{\mathrm{n}})y_{\mathrm{n,i}} \\
&+ 2\lambda p_{\mathrm{q}}(1-\theta)(1-v)(1-\sigma_{\mathrm{v}})y_{\mathrm{v,i}} + \tau y_{\mathrm{n,i}} - \beta y_{\mathrm{n,q}}, \\
\dot{y}_{\mathrm{v,q}} =& 2\lambda(1-\gamma_{\mathrm{t}})p_{\mathrm{q}}(1-\gamma_{\mathrm{q}})v(1-\theta)(1-\sigma_{\mathrm{n}})y_{\mathrm{n,i}} \\
&+ 2\lambda(1-\gamma_{\mathrm{t}})p_{\mathrm{q}}(1-\gamma_{\mathrm{q}})[\theta+v(1-\theta)](1-\sigma_{\mathrm{v}})y_{\mathrm{v,i}} \\
&+ \tau y_{\mathrm{v,i}} - \beta y_{\mathrm{v,q}}. \qquad (27)
\end{aligned}$$

According to standard system-theoretic methods [51], the (local) stability of the DFE is fully determined by the eigenvalues of the Jacobian matrix of (27) evaluated at the origin. After re-sorting the equations in the order $(y_{\mathrm{n,q}}, y_{\mathrm{v,q}}, y_{\mathrm{n,i}}, y_{\mathrm{v,i}})$, we observe that the Jacobian of (27) has the following block-triangular structure:

$$\begin{array}{c} \\ y_{\mathrm{n,q}} \\ y_{\mathrm{v,q}} \\ y_{\mathrm{n,i}} \\ y_{\mathrm{v,i}} \end{array}
\begin{array}{c}
\begin{array}{cccc} y_{\mathrm{n,q}} & y_{\mathrm{v,q}} & y_{\mathrm{n,i}} & y_{\mathrm{v,i}} \end{array} \\
\begin{bmatrix} * & 0 & * & * \\ 0 & * & * & * \\ 0 & 0 & * & * \\ 0 & 0 & * & * \end{bmatrix}
\end{array}, \qquad (28)$$

where an asterisk $(*)$ denotes a nonzero entry.
The block $(y_{\mathrm{n,q}}, y_{\mathrm{v,q}})$ is diagonal and has eigenvalue $\Lambda_{1,2} = -\beta < 0$, with multiplicity 2. Through a direct computation, we establish that the eigenvalues of the block $(y_{\mathrm{n,i}}, y_{\mathrm{v,i}})$ are given by

$$\begin{aligned}
\Lambda_{3,4} =& \lambda\xi - \beta - \tau \\
&\pm \lambda\sqrt{\xi^2 - 4\theta(1-\gamma_{\mathrm{t}})(1-p_{\mathrm{q}})[1-p_{\mathrm{q}}(1-\gamma_{\mathrm{q}})](1-\sigma_{\mathrm{n}})(1-\sigma_{\mathrm{v}})},
\end{aligned}$$

with ξ defined as in (20). Observe that

$$\begin{aligned}
&\xi^2 - 4\theta(1-\gamma_{\mathrm{t}})(1-p_{\mathrm{q}})[1-p_{\mathrm{q}}(1-\gamma_{\mathrm{q}})](1-\sigma_{\mathrm{n}})(1-\sigma_{\mathrm{v}}) \\
&= \theta^2\left[v\rho + (1-v)\phi\right]^2 + 2\theta\left[v(1-v)(\phi-\rho)^2 - \phi\rho\right] \\
&\quad + \left[(1-v)\rho + v\phi\right]^2, \qquad (29)
\end{aligned}$$

where the right-hand side is a polynomial in θ, with

$$\begin{aligned}
\phi &:= (1-\gamma_{\mathrm{t}})[1-p_{\mathrm{q}}(1-\gamma_{\mathrm{q}})](1-\sigma_{\mathrm{v}}), \\
\rho &:= (1-p_{\mathrm{q}})(1-\sigma_{\mathrm{n}}).
\end{aligned}$$

Through explicit computation, we verify that the roots of the right-hand side of Eq. (29) are complex. Since the leading coefficient of the polynomial is positive, it follows that (29) is strictly positive for all θ. Thus, the two eigenvalues $\Lambda_{3,4}$ are real, and the DFE is locally asymptotically stable if and only if the maximum eigenvalue (i.e., the one with the positive sign) is negative, which is the case if $\tau > \bar{\tau}$. On the contrary, if $\tau < \bar{\tau}$, then the maximum eigenvalue is positive and the DFE is unstable. □

APPENDIX B
PROOF OF PROPOSITION 6

All the statements are derived from observing the monotonicity properties of (27) with respect to the considered parameters. For p_{q} and γ_{t}, monotonicity holds only for the equations $\dot{y}_{\mathrm{n,i}}$ and $\dot{y}_{\mathrm{v,i}}$, which are the two that determine the stability of the DFE due to the structure of (28). □

APPENDIX C
PROOF OF THEOREM 2

Let Assumption 2 hold, i.e., $\sigma_{\mathrm{v}} = 1$ and $\sigma_{\mathrm{n}} < 1$. Consider the system in (18). Solving the equilibrium condition $\dot{y}_{\mathrm{n,s}} = 0$ gives

$$y_{\mathrm{n,s}} = \frac{\beta(1-v)}{2\lambda(1-\sigma_{\mathrm{n}})(\frac{\theta}{1-v}+1-\theta)y_{\mathrm{n,i}}+\beta}.$$

Subsequently solving $\dot{y}_{\mathrm{n,i}} = 0$ gives $y_{\mathrm{n,i}} = 0$ (which trivially leads to the DFE $(1-v, 0, 0, v, 0, 0)$) or

$$y_{\mathrm{n,i}} = \beta(1-v)\left(\frac{1-p_{\mathrm{q}}}{\beta+\tau} - \frac{1}{2\lambda(1-\sigma_{\mathrm{n}})[\theta+(1-\theta)(1-v)]}\right),$$

which gives the EE in (25) by solving $\dot{y}_{\mathrm{v,s}} = 0$ and $\dot{y}_{\mathrm{v,i}} = 0$, while noting that $y_{\mathrm{n,q}} = 1 - v - y_{\mathrm{n,s}} - y_{\mathrm{n,i}}$ and $y_{\mathrm{v,q}} = v - y_{\mathrm{v,s}} - y_{\mathrm{v,i}}$. Note that for the EE to exist, we need that $y_{\mathrm{n,i}} > 0$, which is equivalent to the condition $\tau < \hat{\tau}$. Concerning the stability, local stability for the DFE immediately follows from Theorem 1. Now consider the EE in (25), where we assume that $\tau < \hat{\tau}$. Linearizing around the EE, we obtain a Jacobian matrix with eigenvalues

$$\Upsilon_1 = -(\beta + \tau) < 0,$$
$$\Upsilon_2 = -\beta[1 + 2\lambda\kappa(1-\sigma_{\mathrm{n}})(1-\gamma_{\mathrm{t}})(1-\theta)] < 0,$$

and

$$\Upsilon_{3,4} = \tfrac{1}{2}\left(1 - \tfrac{2\lambda(1-\sigma_{\mathrm{n}})[\theta+(1-\theta)(1-v)](1-p_{\mathrm{q}})}{\beta+\tau}\right) \pm \tfrac{1}{2}\sqrt{\left(1-\tfrac{2\lambda(1-\sigma_{\mathrm{n}})[\theta+(1-\theta)(1-v)](1-p_{\mathrm{q}})}{\beta+\tau}\right)^2 - 4[2\lambda(1-\sigma_{\mathrm{n}})[\theta+(1-\theta)(1-v)](1-p_{\mathrm{q}}) - (\beta+\tau)]}.$$

Note that $\tau < \hat{\tau}$ implies that $\mathrm{Re}(\Upsilon_{3,4}) < 0$, so the EE is locally asymptotically stable. □

APPENDIX D
DETAILS ON NUMERICAL SIMULATIONS

The epidemic threshold is estimated as follows. We set a range of values for the parameter τ. For each value of τ, we initialize the epidemics with 10 infected individuals, and we estimate the probability that the disease is extinguished within a fixed time horizon (we set it to $t = 200$) through 10 independent Monte Carlo simulations. Following [52], [53], we estimate the threshold by the value of τ that maximizes the standard deviation of the eradication probability. Because the output of each simulation is a binary variable ('0' for eradication, '1' for endemicity), the value of τ that maximizes the standard deviation coincides with the value that has an estimated eradication probability close to 0.5. To optimize the process, we adopt a two-step procedure. First, we consider a wide range of values of τ with a large step size $\Delta\tau$. We estimate the eradication probability by starting at a high value of τ and decreasing it until we reach a value $\tilde{\tau}$ with an estimated eradication probability of less than 0.5. Second, we use the proposed algorithm to approximate the threshold value in the range $\tau \in [\tilde{\tau} - \Delta\tau, \tilde{\tau} + \Delta\tau]$ with a smaller step size. The code used for all our simulations is available at https://github.com/lzino90/vaccine_siq.

REFERENCES

[1] K. Frieswijk, L. Zino, and M. Cao, "Modelling the effect of vaccination and human behaviour on the spread of epidemic diseases on temporal networks," in *2022 Eur. Control Conf.*, pp. 2291–2296, 2022.

[2] World Health Organization, "Draft landscape and tracker of COVID-19 candidate vaccines." https://www.who.int/publications/m/item/draft-landscape-of-covid-19-candidate-vaccines, 2022.

[3] J. Tang *et al.*, "Respiratory mucosal immunity against SARS-CoV-2 following mRNA vaccination," *Sci. Immunol.*, p. eadd4853, 2022.

[4] K. J. Siddle *et al.*, "Transmission from vaccinated individuals in a large SARS-CoV-2 delta variant outbreak," *Cell*, vol. 185, no. 3, pp. 485–492, 2022.

[5] R. Pastor-Satorras, C. Castellano, P. Van Mieghem, and A. Vespignani, "Epidemic processes in complex networks," *Rev. Mod. Phys.*, vol. 87, pp. 925–979, Aug 2015.

[6] C. Nowzari, V. M. Preciado, and G. J. Pappas, "Analysis and control of epidemics: A survey of spreading processes on complex networks," *IEEE Control Syst. Mag.*, vol. 36, no. 1, pp. 26–46, 2016.

[7] W. Mei, S. Mohagheghi, S. Zampieri, and F. Bullo, "On the dynamics of deterministic epidemic propagation over networks," *Annu. Rev. Control*, vol. 44, pp. 116–128, 2017.

[8] P. E. Paré, C. L. Beck, and T. Başar, "Modeling, estimation, and analysis of epidemics over networks: An overview," *Annu. Rev. Control*, vol. 50, pp. 345–360, 2020.

[9] L. Zino and M. Cao, "Analysis, prediction, and control of epidemics: A survey from scalar to dynamic network models," *IEEE Circ. Syst. Mag.*, vol. 21, no. 4, pp. 4–23, 2021.

[10] B. Qu and H. Wang, "SIS epidemic spreading with heterogeneous infection rates," *IEEE Trans. Netw. Sci.*, vol. 4, no. 3, pp. 177–186, 2017.

[11] F. Fagnani and L. Zino, "Time to extinction for the SIS epidemic model: New bounds on the tail probabilities," *IEEE Trans. Netw. Sci. Eng.*, vol. 6, no. 1, pp. 74–81, 2019.

[12] B. Prasse and P. V. Mieghem, "The viral state dynamics of the discrete-time NIMFA epidemic model," *IEEE Trans. Netw. Sci.*, vol. 7, no. 3, pp. 1667–1674, 2020.

[13] K. Drakopoulos, A. Ozdaglar, and J. N. Tsitsiklis, "An efficient curing policy for epidemics on graphs," *IEEE Trans. Netw. Sci.*, vol. 1, no. 2, pp. 67–75, 2014.

[14] F. D. Sahneh, A. Vajdi, J. Melander, and C. M. Scoglio, "Contact adaption during epidemics: A multilayer network formulation approach," *IEEE Trans. Netw. Sci. Eng.*, vol. 6, no. 1, pp. 16–30, 2017.

[15] V. M. Preciado, M. Zargham, C. Enyioha, A. Jadbabaie, and G. Pappas, "Optimal vaccine allocation to control epidemic outbreaks in arbitrary networks," in *52nd IEEE Conf. Decis. Control*, pp. 7486–7491, 2013.

[16] J. N. Tetteh, V. K. Nguyen, and E. A. Hernandez-Vargas, "Network models to evaluate vaccine strategies towards herd immunity in COVID-19," *J. Theor. Biol.*, vol. 531, p. 110894, Dec. 2021.

[17] C. Bongiorno and L. Zino, "A multi-layer network model to assess school opening policies during a vaccination campaign: a case study on COVID-19 in France," *Appl. Netw. Sci.*, vol. 7, no. 1, p. 12, 2022.

[18] F. Parino, L. Zino, M. Porfiri, and A. Rizzo, "Modelling and predicting the effect of social distancing and travel restrictions on COVID-19 spreading," *J. R. Soc. Interface*, vol. 18, no. 175, p. 20200875, 2021.

[19] R. Carli, G. Cavone, N. Epicoco, P. Scarabaggio, and M. Dotoli, "Model predictive control to mitigate the COVID-19 outbreak in a multi-region scenario," *Annu. Rev. Control*, vol. 50, pp. 373–393, 2020.

[20] F. Della Rossa *et al.*, "A network model of Italy shows that intermittent regional strategies can alleviate the COVID-19 epidemic," *Nat. Comm.*, vol. 11, no. 1, p. 5106, 2020.

[21] Y.-C. Chen, P.-E. Lu, C.-S. Chang, and T.-H. Liu, "A time-dependent SIR model for COVID-19 with undetectable infected persons," *IEEE Trans. Netw. Sci. Eng.*, vol. 7, no. 4, pp. 3279–3294, 2020.

[22] N. Perra, B. Gonçalves, R. Pastor-Satorras, and A. Vespignani, "Activity driven modeling of time varying networks," *Sci. Rep.*, vol. 2, p. 469, 2012.

[23] L. Zino, A. Rizzo, and M. Porfiri, "Continuous-time discrete-distribution theory for activity-driven networks," *Phys. Rev. Lett.*, vol. 117, no. 228302, 2016.

[24] A. Bessi *et al.*, "Homophily and polarization in the age of misinformation," *Eur. Phys. J.: Spec. Top.*, vol. 225, pp. 2047–2059, Oct 2016.

[25] A. L. Schmidt, F. Zollo, A. Scala, C. Betsch, and W. Quattrociocchi, "Polarization of the vaccination debate on Facebook," *Vaccine*, vol. 36, no. 25, pp. 3606–3612, 2018.

[26] B. Mønsted and S. Lehmann, "Characterizing polarization in online vaccine discourse—a large-scale study," *PloS one*, vol. 17, no. 2, p. e0263746, 2022.

[27] S. Rathje, J. K. He, J. Roozenbeek, J. J. Van Bavel, and S. van der Linden, "Social media behavior is associated with vaccine hesitancy," *PNAS Nexus*, vol. 1, 09 2022.

[28] P. Van Mieghem, J. Omic, and R. Kooij, "Virus spread in networks," *IEEE/ACM Trans. Netw.*, vol. 17, no. 1, pp. 1–14, 2009.

[29] L. Zino, A. Rizzo, and M. Porfiri, "On assessing control actions for epidemic models on temporal networks," *IEEE Control Syst. Lett.*, vol. 4, no. 4, pp. 797–802, 2020.

[30] N. T. J. Bailey, *The elements of stochastic processes with applications to the natural sciences*, vol. 25. John Wiley & Sons, 1991.
[31] D. A. Levin, Y. Peres, and E. L. Wilmer, *Markov chains and mixing times*. Providence RI, US: American Mathematical Society, 2006.
[32] L. Zino, A. Rizzo, and M. Porfiri, "An analytical framework for the study of epidemic models on activity driven networks," *J. Complex Netw.*, vol. 5, no. 6, pp. 924–952, 2017.
[33] L. Zino, A. Rizzo, and M. Porfiri, "The impact of deniers on epidemics: A temporal network model," *IEEE Control Syst. Lett.*, vol. 7, pp. 685–690, 2023.
[34] M. Grottke, A. Avritzer, D. S. Menasché, L. P. de Aguiar, and E. Altman, "On the efficiency of sampling and countermeasures to critical-infrastructure-targeted malware campaigns," *SIGMETRICS Perform. Eval. Rev.*, vol. 43, p. 33–42, feb 2016.
[35] G. Giordano *et al.*, "Modelling the COVID-19 epidemic and implementation of population-wide interventions in Italy," *Nat. Med.*, vol. 26, pp. 855–860, 2020.
[36] W. Xuan, R. Ren, P. E. Paré, M. Ye, S. Ruf, and J. Liu, "On a network SIS model with opinion dynamics," in *21st IFAC World Congress*, vol. 53, pp. 2582–2587, 2020.
[37] B. She, J. Liu, S. Sundaram, and P. E. Pare, "On a networked SIS epidemic model with cooperative and antagonistic opinion dynamics," *IEEE Trans. Control Netw. Syst.*, pp. 1–1, 2022.
[38] M. Ye, L. Zino, A. Rizzo, and M. Cao, "Game-theoretic modeling of collective decision making during epidemics," *Phys. Rev. E*, vol. 104, p. 024314, 2021.
[39] A. R. Hota, T. Sneh, and K. Gupta, "Impacts of game-theoretic activation on epidemic spread over dynamical networks," *SIAM J. Control Optim.*, vol. 60, no. 2, pp. S92–S118, 2022.
[40] K. Frieswijk, L. Zino, M. Ye, A. Rizzo, and M. Cao, "A mean-field analysis of a network behavioral–epidemic model," *IEEE Control Syst. Lett.*, vol. 6, pp. 2533–2538, 2022.
[41] E. Altman, M. Datar, F. de Pellegrini, S. Perlaza, and D. S. Menasché, "The mask game with multiple populations," *Dyn. Games Appl.*, vol. 12, no. 1, pp. 147–167, 2022.
[42] T. G. Kurtz, "Limit theorems for sequences of jump Markov processes approximating ordinary differential processes," *J Appl. Prob.*, vol. 8, no. 2, pp. 344–356, 1971.
[43] T. Ripp and J. P. Röer, "Systematic review on the association of COVID-19-related conspiracy belief with infection-preventive behavior and vaccination willingness," *BMC Psychol.*, vol. 10, no. 1, pp. 1–14, 2022.
[44] C. Phucharoen, N. Sangkaew, and K. Stosic, "The characteristics of COVID-19 transmission from case to high-risk contact, a statistical analysis from contact tracing data," *EClinicalMedicine*, vol. 27, p. 100543, 2020.
[45] N. Dagan *et al.*, "BNT162b2 mRNA Covid-19 vaccine in a nationwide mass vaccination setting," *N. Engl. J. Med.*, vol. 384, no. 15, pp. 1412–1423, 2021.
[46] R. K. Suryawanshi *et al.*, "Limited cross-variant immunity from SARS-CoV-2 omicron without vaccination," *Nature*, vol. 607, no. 7918, pp. 351–355, 2022.
[47] C. T. Bauch and D. J. D. Earn, "Vaccination and the theory of games," *Proc. Natl. Acad. Sci. USA*, vol. 101, no. 36, pp. 13391–13394, 2004.
[48] A. R. Hota and S. Sundaram, "Game-theoretic vaccination against networked SIS epidemics and impacts of human decision-making," *IEEE Trans. Control. Netw. Syst.*, vol. 6, no. 4, pp. 1461–1472, 2019.
[49] X.-J. Li, C. Li, and X. Li, "The impact of information dissemination on vaccination in multiplex networks," *Sci. China Inf. Sci.*, vol. 65, June 2022.
[50] Y. Tatsukawa, M. R. Arefin, S. Utsumi, and J. Tanimoto, "Investigating the efficiency of dynamic vaccination by consolidating detecting errors and vaccine efficacy," *Sci. Rep.*, vol. 12, no. 1, 2022.
[51] W. J. Rugh, *Linear System Theory*. London, UK: Pearson, 2 ed., 1996.
[52] A. Moinet, R. Pastor-Satorras, and A. Barrat, "Effect of risk perception on epidemic spreading in temporal networks," *Phys. Rev. E*, vol. 97, p. 012313, Jan 2018.
[53] L. Zino, A. Rizzo, and M. Porfiri, "Modeling memory effects in activity-driven networks," *SIAM J. Appl. Dyn. Syst.*, vol. 17, pp. 2830–2854, Jan. 2018.

Kathinka Frieswijk is a PhD candidate at the Faculty of Science and Engineering, University of Groningen (UG), the Netherlands. At the UG, she received a BS in Medicine, a BS in Mathematics, and a BS in Physics, and she graduated in 2018 with an MS in Theoretical Physics. In 2022, she received a Fulbright scholarship (as well as scholarships from Stichting Het Scholten-Cordes Fonds and dr. Hendrik Mullerfonds) to conduct research at Yale University, New Haven, CT, USA. Her research interests include opinion dynamics (focusing on climate change in particular), epidemic modeling on large-scale networks, and evolutionary game theory.

Lorenzo Zino has been an Assistant Professor with the Department of Electronics and Telecommunications at Politecnico di Torino (Turin, Italy) since 2022. He received the BS in Applied Mathematics and MS in Mathematical Engineering (summa cum laude) from Politecnico di Torino, Torino, Italy, in 2012 and 2014, respectively, and the PhD in Pure and Applied Mathematics (with honors) from Politecnico di Torino and Università di Torino (joint doctorate program), in 2018. He was a Research Fellow at Politecnico di Torino (2018–19) and the University of Groningen (2019–22) and a Visiting Research Assistant at New York University Tandon School of Engineering (2017–18 and 2019). His current research interests include modeling, analysis, and control of dynamics over complex networks, applied probability, network analysis, and game theory. Since 2021, he has been an Associate Editor of the *Journal of Computational Science*.

Ming Cao received bachelor's and master's degrees from Tsinghua University, Beijing, China, in 1999 and 2002, respectively, and a Ph.D. degree from Yale University, New Haven, CT, USA, in 2007, all in electrical engineering. Since 2016, he has been a Professor of systems and control with the Engineering and Technology Institute, the University of Groningen, the Netherlands, where he started as a tenure-track Assistant Professor in 2008. From September 2007 to August 2008, he was a Postdoctoral Research Associate with the Department of Mechanical and Aerospace Engineering, Princeton University, Princeton, NJ, USA. He was a research intern during the summer of 2006 with the Mathematical Sciences Department, the IBM T. J. Watson Research Center, NY, USA. His research interests include autonomous agents and multi-agent systems, complex networks, and decision-making processes. Prof. Cao is the 2017 and inaugural recipient of the Manfred Thoma Medal from IFAC and the 2016 recipient of the European Control Award sponsored by the European Control Association. He is a Senior Editor for Systems and Control Letters, and an Associate Editor for IEEE Transactions on Automatic Control; he was an associate editor for IEEE Transactions on Circuits and Systems, and IEEE Circuits and Systems Magazine. He is a Vice Chair of the IFAC Technical Committee on Large-Scale Complex Systems.